

Data-driven Bayesian State Estimation with Compressed Measurement of Model-free Process using Semi-supervised Learning

Anubhab Ghosh *, Yonina C. Eldar †, Saikat Chatterjee *

* Digital Futures Centre and School of Elect. Engg. & Comp. Sc., KTH Royal Institute of Technology, Sweden

† Faculty of Mathematics and Computer Science, The Weizmann Institute of Science, Israel

* anubhabg@kth.se, † yonina.eldar@weizmann.ac.il, * sach@kth.se

Abstract—The research topic is: data-driven Bayesian state estimation with compressed measurement (BSCM) of model-free process, say for a (causal) tracking application. The dimension of the temporal measurement vector is lower than the dimension of the temporal state vector to be estimated. Hence the state estimation problem is an underdetermined inverse problem. The state-space-model (SSM) of the underlying dynamical process is assumed to be unknown and hence, we use the terminology ‘model-free process’. In absence of the SSM, we can not employ traditional model-driven methods like Kalman Filter (KF) and Particle Filter (PF), and instead require data-driven methods. We first experimentally show that two existing unsupervised learning-based data-driven methods fail to address the BSCM problem for model-free process; they are – data-driven nonlinear state estimation (DANSE) method and deep Markov model (DMM) method. The unsupervised learning uses unlabelled data comprised of only noisy measurements. While DANSE provides a good predictive / forecasting performance to model the temporal measurement data as time-series, its unsupervised learning lacks a regularization for state estimation. We then investigate use of a semi-supervised learning approach, and develop a semi-supervised learning-based DANSE method, referred to as SemiDANSE. In the semi-supervised learning, we use a limited amount of labelled data along-with a large amount of unlabelled data, and that helps to bring the desired regularization for BSCM problem in the absence of SSM. The labelled data means pairwise measurement-and-state data. Using three chaotic dynamical systems (or processes) with nonlinear SSMs as benchmark, we show that the data-driven SemiDANSE provides competitive performance for BSCM against three SSM-informed methods - a hybrid method called KalmanNet, and two traditional model-driven methods called extended KF (EKF) and unscented KF (UKF).

Index Terms—Bayesian state estimation, semi-supervised learning, maximum-likelihood, recurrent neural network.

I. INTRODUCTION

Bayesian State estimation with Compressed Measurement: Using a discrete time index t , let there be a nonlinear dynamical process $\{\mathbf{x}_t\}$ generating a sequence $\mathbf{x}_1, \mathbf{x}_2, \dots, \mathbf{x}_t, \dots$, where the m -dimensional state $\mathbf{x}_t \in \mathbb{R}^m$ is observed using an n -dimensional noisy linear measurement $\mathbf{y}_t \in \mathbb{R}^n$, as follows.

$$\text{Linear measurement: } \mathbf{y}_t = \mathbf{H}\mathbf{x}_t + \mathbf{w}_t, \quad t = 1, 2, \dots, \quad (1)$$

This work has been submitted to the IEEE for possible publication. Copyright may be transferred without notice, after which this version may no longer be accessible. The work is supported by a research grant from Digital Futures Centre. Project title: “DLL: Data-limited learning of complex systems”. Website: <https://www.digitalfutures.kth.se/>

where $\mathbf{w}_t \sim \mathcal{N}(\mathbf{w}_t; \mathbf{0}, \mathbf{C}_w)$ is a Gaussian measurement noise with zero mean and covariance \mathbf{C}_w , and $\mathbf{H} \in \mathbb{R}^{n \times m}$ denotes the measurement system. For the measurement system, \mathbf{H} and \mathbf{C}_w are assumed to be known. The Bayesian state estimation task is to find the posterior $p(\mathbf{x}_t | \mathbf{y}_t, \mathbf{y}_{t-1}, \dots, \mathbf{y}_1), t = 1, 2, \dots$, causally.

Our focus is the setup when $n < m$ (compressed measurement), and there is no state-space model (SSM) of the process $\{\mathbf{x}_t\}$. The process is ‘model-free’ due to the absence of the knowledge of the SSM. Estimating the posterior of the model-free process with $n < m$ is an under-determined state estimation problem. This we refer to as the ‘Bayesian State estimation with Compressed Measurement’ (BSCM) problem, where the measurement matrix \mathbf{H} is fat. A fat \mathbf{H} matrix, by appropriate structure, can subsume the special case of partial measurements, that means when n components of the m -dimensional \mathbf{x}_t are observed. Here we mention that, even when the setup is not under-determined, that means if $n \geq m$, the Bayesian state estimation task for a model-free process is non-trivial.

If SSM is available, or sparsity could be exploited: If SSM is available, then the traditional methods to address the BSCM problem are the SSM-informed model-driven methods - Kalman filter (KF) and its extensions such as extended KF (EKF), unscented KF (UKF), and sampling-based particle filter (PF) [1]–[5]. Typically, an SSM is constructed using the physics of the underlying process. For example, KF uses a linear SSM and EKF uses a linearized SSM. Note that we do not have an SSM for a model-free process, and hence we can not use KF and PF for the BSCM problem.

To handle a compressed measurement setup (1), a much-cited approach in signal processing and machine learning is exploitation of sparsity as regularization. If \mathbf{x}_t has sparsity, then the use of ‘sparse representations’, ‘sparse models’, and ‘compressive sensing’ could be explored [6], and combined with traditional KF variants [7], [8] or iterative approaches [9]. Note that the notion of ‘sparsity’ exists when we have an underlying signal model, and here we are dealing with model-free process. Hence, the scope of exploiting sparsity to address the BSCM problem does not arise in this article.

Data-driven methods: To address the BSCM problem with model-free process we require to use data-driven methods, for example, recurrent neural network (RNN) based methods

[10]–[14]. Data-driven methods use training data for learning. From a learning perspective, supervised learning using labelled data would be expected to perform satisfactorily, but it would be interesting if unsupervised learning using unlabelled data could also perform well.

By unlabelled training data, we mean that the training data is comprised of a set of measurements $\{y_t\}$, but no $\{x_t\}$. While a collection of a sufficient amount of unlabelled training data is realistic, for example, by observing a model-free process for a long period, it is costly to collect a sufficient amount of labelled data ($\{y_t\}, \{x_t\}$). Hence, designing a fully supervised learning-based method is challenging.

Limitation of unsupervised learning for BSCM: Recently, an unsupervised learning-based data-driven nonlinear state estimation (DANSE) method for model-free process was proposed [15], [16]. DANSE performs well when the measurement vector is not compressed in (1), and hence the state estimation problem is not under-determined. For $n = m$, DANSE was shown to provide satisfactory performance and remain competitive with SSM-informed EKF, UKF, a hybrid method called KalmanNet [17] and a data-driven deep Markov model (DMM) method [13]. The KalmanNet is an SSM-informed data-driven method.

In the same article [16], it was shown that DANSE is unable to address the BSCM problem ($n < m$) using a Lorenz-63 system as underlying process (see section III. F of [16]). The study leads to a natural *hypothesis*: an unsupervised learning-based data-driven method, like DANSE, can not address the BSCM problem. In [16] there was no comprehensive study to verify the hypothesis, and hence we pursue further for addressing this limitation of unsupervised learning.

Research questions: To address the BSCM problem for model-free process, we raise the following research questions.

- 1) Do there exist unsupervised learning-based methods to address the BSCM problem for a model-free process?
- 2) If unsupervised learning has the limitation then can we design a semi-supervised learning-based method? Semi-supervised learning uses a limited amount of labelled data along-with a sufficient amount of unlabelled data.

Our contributions:

- 1) To address the first research question, we start with an argument. A model-free (nonlinear) dynamical process $\{x_t\}$ has statistical relations between state vectors x_t across t . In absence of an SSM, it is a nontrivial task to capture the statistical relations using measurements $\{y_t\}$. While we do not have a theory to justify that there exists no unsupervised learning method to exploit the statistical relations, we perform experiments to show the limitation of unsupervised learning-based methods. For the experiment we use two existing unsupervised learning-based methods - DANSE and DMM - and show both of them are unable to address the BSCM problem. This is experimentally demonstrated using a benchmark chaotic dynamical process - a Lorenz-63 system [18].
- 2) To address the second question, we develop a semi-supervised learning-based method, referred to as semi-supervised DANSE (SemiDANSE). Along-with Lorenz-63 system we also performed experiments using two

other chaotic dynamical systems - a Chen system [19], [20] and a Rössler system [21]. We show DANSE fails, but SemiDANSE performs well for the BSCM problem.

A. Relevant Literature Review

In this subsection, we provide concise reviews for brevity.

Bayesian state estimation: We begin with recent advances in the field of data-driven Bayesian state estimation. Note that we have already referred to the major model-driven methods such as KF, EKF and UKF, and the data-driven methods such as DANSE and DMM. Further examples of data-driven methods are Gaussian process-based (GP-based) methods such as [22]–[24] that seek to learn the underlying process dynamics in a data-driven manner [11], [25]. A second approach involves learning an inverse of the measurement model in (1) and performing inference using message passing and graph neural networks in [26]. Another class of methods involves the use of model-driven with data-driven approaches, e.g. using a UKF with RNNs to model the process state dynamics with a general non-linear autoregressive moving-average (NARMA) model [27] or relaxing the Markovian constraint of KF in the process state dynamics and using long short-term memory networks (LSTMs) for learning the process state dynamics using linear measurements as proposed in [28]. There also exists a semi-supervised approach using differentiable particle filters to explicitly learning state dynamics and a measurement model, applied to localization tasks as proposed in [29]. Finally, similar to DMM, there exist other variational inference-based approaches such as dynamic variational autoencoders (DVAEs) [12]–[14], [30].

We mention that a more comprehensive review of Bayesian state estimation covering model-driven, data-driven and hybrid paradigms can be found in [16, section I-A.]. The hybrid methods combine model-driven methods with data-driven techniques, The prominent hybrid method is KalmanNet that we already referred [17]. KalmanNet is SSM-informed and it uses power of data-driven neural networks.

Semi-supervised learning: We now provide a brief review of semi-supervised learning as it is used for SemiDANSE. The field of semi-supervised learning has been well-studied [31], [32]. Typically, semi-supervised learning is utilized in scenarios where labelled data is insufficient to achieve good performance, for examples, classification, regression, clustering, etc. Introductory and comprehensive early texts on the subject can be found in [33], [34], where the authors explain the general setting of semi-supervised learning. An interesting and difficult question is usually “When is semi-supervised learning effective?”. In general, it can be quite challenging to answer the question, and continues to be an area of research [31]. We also find that a large body of research works in the semi-supervised learning, described in recent survey papers [31], [32], predominantly considers classification tasks, while there is comparatively a limited amount of work that considers regression tasks [35]. Note that Bayesian state estimation and the BSCM problem are regression tasks.

B. Notations and Outline of the paper

We use bold font lowercase symbols to denote vectors and regular lowercase font to denote scalars, for example, \mathbf{x} represents a vector while x_j represents the j 'th component of \mathbf{x} . A sequence of vectors $\mathbf{x}_1, \mathbf{x}_2, \dots, \mathbf{x}_t$ is compactly denoted by $\mathbf{x}_{1:t}$, where t denotes a discrete time index. Then $x_{t,j}$ denotes the j 'th component of \mathbf{x}_t . Upper case symbols in bold font, like \mathbf{H} , represent matrices. The operator $(\cdot)^\top$ denotes the transpose. $\mathcal{N}(\cdot; \mathbf{m}, \mathbf{L})$ represents the probability density function of the Gaussian distribution with mean \mathbf{m} and covariance matrix \mathbf{L} . $\det(\cdot)$, $\mathbb{E}[\cdot]$ and $\text{tr}(\cdot)$ denote the determinant, expectation, and the trace operator respectively. The notation $\|\mathbf{x}\|_{\mathbf{C}}^2$ denotes the squared ℓ_2 norm of \mathbf{x} weighted by the matrix \mathbf{C} , i.e. $\|\mathbf{x}\|_{\mathbf{C}}^2 = \mathbf{x}^\top \mathbf{C} \mathbf{x}$. $\text{diag}(\mathbf{x})$ denotes a square, diagonal matrix with \mathbf{x} in its main diagonal. $|\mathcal{D}|$ denotes the cardinality of the set \mathcal{D} . $\exp(\mathbf{A})$ denotes the matrix exponential of the matrix \mathbf{A} . We mention that our notations are similar to that in [16].

The outline of the paper is as follows: in section II we formulate the SemiDANSE. Then we perform experiments in section III to show how SemiDANSE can be used for addressing the BSCM problem and compare its performance with relevant model-driven, data-driven and hybrid methods. Finally, we provide our conclusions and final remarks in section IV.

II. SEMIDANSE

In this section, we develop the SemiDANSE method. We first start with the inference problem - the estimation problem. Then we address the learning problem. We also provide some thoughts on the unsupervised learning task and how SemiDANSE addresses this problem.

A. Inference problem - the posterior estimation

At the onset of this subsection, we mention the contents of this subsection II-A have a considerable similarity with that of [16, section II-B]. We provide this subsection for completeness and ease of readability of this article.

Like DANSE, for the proposed SemiDANSE, an RNN recursively uses $\mathbf{y}_{1:t-1}$ as input sequence and provide parameters of a Gaussian prior for \mathbf{x}_t as $p(\mathbf{x}_t | \mathbf{y}_{1:t-1})$. This is schematically shown in Fig. 2. The RNN (together with the feed-forward networks) has learnable parameters denoted by θ . The actual RNN that we used is a GRU [36]. A brief discussion about our GRU implementation including its layers are explained later in section III-B1 and Appendix A.

Then, using the linear measurement setup (1), we can compute the posterior $p(\mathbf{x}_t | \mathbf{y}_{1:t})$ in closed-form Gaussian distribution.

$$\begin{aligned} \text{Prior : } p(\mathbf{x}_t | \mathbf{y}_{1:t-1}) &= \mathcal{N}(\mathbf{x}_t; \mathbf{m}_{t|1:t-1}(\theta), \mathbf{L}_{t|1:t-1}(\theta)), \\ \text{such that } \{\mathbf{m}_{t|1:t-1}(\theta), \mathbf{L}_{t|1:t-1}(\theta)\} &\triangleq \boldsymbol{\alpha}_{t|1:t-1}(\theta), \\ \boldsymbol{\alpha}_{t|1:t-1}(\theta) &= \text{RNN}(\mathbf{y}_{1:t-1}; \theta). \\ \text{Observation : } p(\mathbf{y}_t | \mathbf{x}_t) &= \mathcal{N}(\mathbf{y}_t; \mathbf{H}\mathbf{x}_t, \mathbf{C}_w). \end{aligned} \quad (2)$$

Here, $\mathbf{m}_{t|1:t-1}(\theta) \in \mathbb{R}^m$ and $\mathbf{L}_{t|1:t-1}(\theta) \in \mathbb{R}^{m \times m}$ denote the mean and covariance matrix of the Gaussian prior distribution, respectively. The mean and covariance depend on θ , and hence

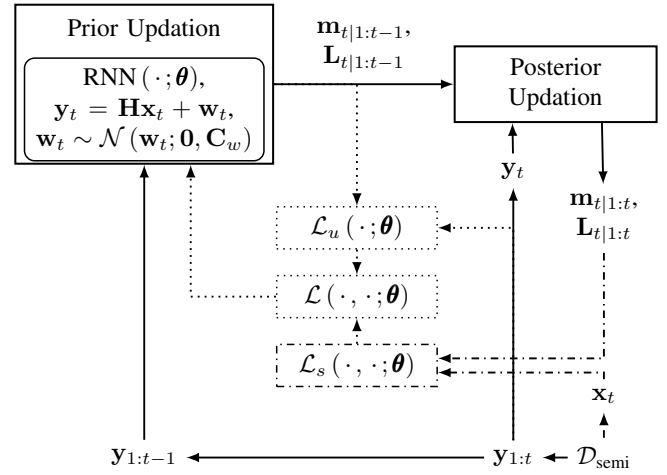


Fig. 1: Schematic of SemiDANSE at the t 'th time instant. The dotted lines represent information flow specifically during the learning phase, i.e. calculation of losses and gradients for RNN learning, $\mathcal{D}_{\text{semi}}$ represents the training dataset for SemiDANSE as defined in (10), \mathcal{L}_s and \mathcal{L}_u denote the supervised and the unsupervised loss respectively at the t 'th instant as defined in (19) and (20) respectively. The dash-dotted lines denote information flow specifically involving the limited \mathcal{D}_s in $\mathcal{D}_{\text{semi}}$ during the learning phase. Solid lines represent information flow involving other quantities and during inference.

we show it in notations. We use $\mathbf{L}_{t|1:t-1}(\theta)$ as a diagonal covariance matrix for ease of practical implementation. Then, using the 'completing the square' approach [37, Chap. 2], the posterior distribution of the current state $p(\mathbf{x}_t | \mathbf{y}_{1:t})$ is obtained in closed-form as

$$\begin{aligned} p(\mathbf{x}_t | \mathbf{y}_{1:t}) &= \mathcal{N}(\mathbf{x}_t; \mathbf{m}_{t|1:t}(\theta), \mathbf{L}_{t|1:t}(\theta)), \\ \mathbf{m}_{t|1:t}(\theta) &= \mathbf{m}_{t|1:t-1}(\theta) + \mathbf{K}_{t|1:t-1} \boldsymbol{\varepsilon}_t, \\ \mathbf{L}_{t|1:t}(\theta) &= \mathbf{L}_{t|1:t-1}(\theta) - \mathbf{K}_{t|1:t-1} \mathbf{R}_{\varepsilon,t} \mathbf{K}_{t|1:t-1}^\top, \end{aligned} \quad (3)$$

where the second equation in (3) is obtained using the Woodbury matrix identity/matrix inversion lemma, with

$$\begin{aligned} \mathbf{K}_{t|1:t-1} &\triangleq \mathbf{L}_{t|1:t-1}(\theta) \mathbf{H}^\top \mathbf{R}_{\varepsilon,t}^{-1}, \\ \mathbf{R}_{\varepsilon,t} &\triangleq \mathbf{H} \mathbf{L}_{t|1:t-1}(\theta) \mathbf{H}^\top + \mathbf{C}_w, \text{ and} \\ \boldsymbol{\varepsilon}_t &\triangleq \mathbf{y}_t - \mathbf{H} \mathbf{m}_{t|1:t-1}(\theta). \end{aligned} \quad (4)$$

A point estimate can be $\mathbf{m}_{t|1:t}(\theta)$, that provides a practical mean-square-error (MSE) performance as $\mathbb{E}[\|\mathbf{x}_t - \mathbf{m}_{t|1:t}(\theta)\|_2^2] = \text{tr}(\mathbf{L}_{t|1:t}(\theta))$.

In addition, if we are interested to find out $p(\mathbf{x}_{1:t} | \mathbf{y}_{1:t})$, we use the following assumption mentioned in [16] as follows:

Assumption 1. As we neither have an SSM for the model-free process $\{\mathbf{x}_t\}$ and nor access to the true states $\mathbf{x}_t, \forall t$, during inference, we assume

$$p(\mathbf{x}_t | \mathbf{y}_{1:t}, \mathbf{x}_{1:t-1}) = p(\mathbf{x}_t | \mathbf{y}_{1:t}). \quad (5)$$

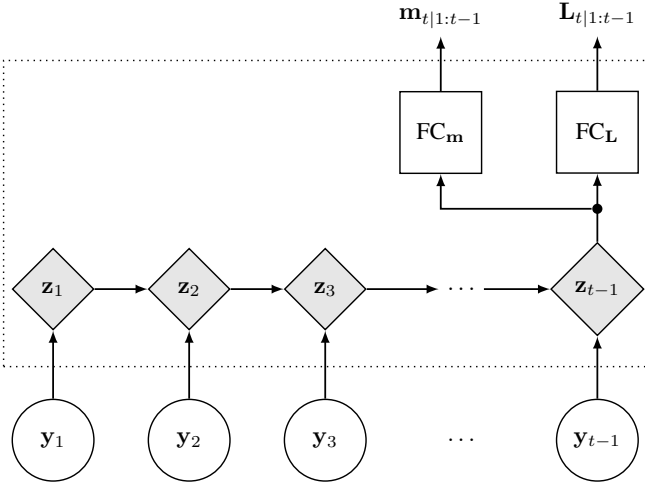


Fig. 2: Schematic of the parameterization of the Gaussian prior $p(\mathbf{x}_t|\mathbf{y}_{1:t-1})$ in (2) using an RNN (unfolded in time). The input to the RNN is the sequence $\mathbf{y}_{1:t-1}$ (unshaded, circle nodes). The internal states of the RNN are $\{\mathbf{z}_\tau\}$ (shaded, diamond nodes). At the last time instant the hidden state \mathbf{z}_{t-1} is mapped to $\mathbf{m}_{t|1:t-1}$ and $\mathbf{L}_{t|1:t-1}$ of the Gaussian prior using shallow feed-forward networks with suitable activation functions denoted by FC_m and FC_L respectively. The mathematical details of the RNN and the feed-forward networks are described in Appendix A.

Using (3) and assumption 1, we write the joint posterior as

$$\begin{aligned}
 p(\mathbf{x}_{1:t}|\mathbf{y}_{1:t}) &= p(\mathbf{x}_t|\mathbf{y}_{1:t}, \mathbf{x}_{1:t-1})p(\mathbf{x}_{1:t-1}|\mathbf{y}_{1:t}) \\
 &= p(\mathbf{x}_t|\mathbf{y}_{1:t})p(\mathbf{x}_{1:t-1}|\mathbf{y}_{1:t-1}) \\
 &= \prod_{\tau=1}^t p(\mathbf{x}_\tau|\mathbf{y}_{1:\tau}) \\
 &= \prod_{\tau=1}^t \mathcal{N}(\mathbf{x}_\tau; \mathbf{m}_{\tau|1:\tau}(\boldsymbol{\theta}), \mathbf{L}_{\tau|1:\tau}(\boldsymbol{\theta})) \\
 &\triangleq p(\mathbf{x}_{1:t}|\mathbf{y}_{1:t}; \boldsymbol{\theta}).
 \end{aligned} \tag{6}$$

The notation $p(\mathbf{x}_{1:t}|\mathbf{y}_{1:t}; \boldsymbol{\theta})$ is to show the dependency of $p(\mathbf{x}_{1:t}|\mathbf{y}_{1:t})$ on $\boldsymbol{\theta}$.

In the next subsection, we describe the semi-supervised learning of SemiDANSE, which includes learning the parameters $\boldsymbol{\theta}$ of the RNN. Once the learning is completed, SemiDANSE can be readily used for the inference as part of testing phase. Note that, as per conventional practice, inference data samples are not part of learning phase (or training phase).

A schematic diagram of SemiDANSE is depicted in Fig. 1 for visualization of inference and learning. Similar to DANSE, we emphasize the absence of an Gaussian propagation from the posterior to the prior during the learning and inference process.

B. Semi-supervised learning

For semi-supervised learning we expect to have a limited amount of labelled data along-with a sufficient amount of unlabelled data [34]. In the following subsections, we formally describe the training dataset for semi-supervised learning and our maximum-likelihood based learning scheme.

1) *Training data*: Let there be a set of N natural indices denoted by $[N] \triangleq \{1, 2, \dots, N\}$. Suppose we have two disjoint subsets of indices as $\mathcal{I}_s \subseteq [N]$ and $\mathcal{I}_u \subseteq [N]$, such that

$\mathcal{I}_s \cup \mathcal{I}_u = [N]$ and $\mathcal{I}_s \cap \mathcal{I}_u = \emptyset$. Let us introduce two notations as $N_s \triangleq |\mathcal{I}_s|$ and $N_u \triangleq |\mathcal{I}_u|$, such that $N_s + N_u = N$.

A T -length state sequence $\mathbf{x}_{1:T}$ has its corresponding measurement sequence $\mathbf{y}_{1:T}$. Let us assume that there exists a genie that has access to a dataset

$$\mathcal{D} \triangleq \left\{ \left(\mathbf{x}_{1:T^{(i)}}^{(i)}, \mathbf{y}_{1:T^{(i)}}^{(i)} \right) \right\}_{i \in [N]}, \tag{7}$$

where $T^{(i)}$ is the length of i 'th sequence. The dataset has N independent state-and-measurement pairwise data samples from the joint random process $p(\{\mathbf{x}_t\}, \{\mathbf{y}_t\})$. The genie makes a part of the full dataset \mathcal{D} accessible to a designer. When the genie provides the dataset

$$\mathcal{D}_u \triangleq \left\{ \left(\mathbf{y}_{1:T^{(i)}}^{(i)} \right) \right\}_{i \in \mathcal{I}_u} \subset \mathcal{D} \tag{8}$$

to the designer then the \mathcal{D}_u has unlabelled data as the measurement-only data for unsupervised learning. If $|\mathcal{I}_u| \triangleq N_u = N$ then the designer received maximum amount of unlabelled data. On the other hand, if the genie provides the labelled dataset

$$\mathcal{D}_s = \left\{ \left(\mathbf{x}_{1:T^{(j)}}^{(j)}, \mathbf{y}_{1:T^{(j)}}^{(j)} \right) \right\}_{j \in \mathcal{I}_s} \subseteq \mathcal{D} \tag{9}$$

then the designer can use it for supervised learning. If $|\mathcal{I}_s| \triangleq N_s = N$ then the designer received maximum amount of labelled data. Finally, if we have access to a dataset $\mathcal{D}_{\text{semi}}$ comprised of two parts as

$$\mathcal{D}_{\text{semi}} = \{\mathcal{D}_s, \mathcal{D}_u\}, \tag{10}$$

such that $|\mathcal{I}_s| \triangleq N_s \ll N$ and $|\mathcal{I}_u| \triangleq N_u = N - N_s$, then \mathcal{D}_s is the part of the dataset that is labelled, and \mathcal{D}_u is the part of the dataset that is unlabelled. The dataset $\mathcal{D}_{\text{semi}}$ can be used for semi-supervised learning.

2) Maximum-likelihood based semi-supervised learning:

For semi-supervised learning, we start with

$$\begin{aligned}
 p(\mathbf{x}_{1:t}, \mathbf{y}_{1:t}) &\triangleq p(\mathbf{x}_{1:t}, \mathbf{y}_{1:t}; \boldsymbol{\theta}) \\
 &= p(\mathbf{x}_{1:t}|\mathbf{y}_{1:t}; \boldsymbol{\theta})p(\mathbf{y}_{1:t}; \boldsymbol{\theta}),
 \end{aligned} \tag{11}$$

where the joint distribution of the measurements is as follows:

$$p(\mathbf{y}_{1:t}) \triangleq p(\mathbf{y}_{1:t}; \boldsymbol{\theta}) = \prod_{\tau=1}^t p(\mathbf{y}_\tau|\mathbf{y}_{1:\tau-1}; \boldsymbol{\theta}), \tag{12}$$

and the conditional distribution is expressed as in [16, section II-B]

$$\begin{aligned}
 p(\mathbf{y}_t|\mathbf{y}_{1:t-1}) &= \int_{\mathbf{x}_t} p(\mathbf{y}_t, \mathbf{x}_t|\mathbf{y}_{1:t-1}) d\mathbf{x}_t \\
 &= \int_{\mathbf{x}_t} p(\mathbf{y}_t|\mathbf{x}_t)p(\mathbf{x}_t|\mathbf{y}_{1:t-1}) d\mathbf{x}_t \\
 &= \mathcal{N}(\mathbf{y}_t; \mathbf{H}\mathbf{m}_{t|1:t-1}(\boldsymbol{\theta}), \mathbf{C}_w + \mathbf{H}\mathbf{L}_{t|1:t-1}(\boldsymbol{\theta})\mathbf{H}^\top) \\
 &\triangleq p(\mathbf{y}_t|\mathbf{y}_{1:t-1}; \boldsymbol{\theta}).
 \end{aligned} \tag{13}$$

In the above we used (2). Here we introduced the notation $p(\mathbf{y}_{1:t}; \boldsymbol{\theta})$ to show the dependency of $p(\mathbf{y}_{1:t})$ on $\boldsymbol{\theta}$. Note that (13) is a predictive distribution of \mathbf{y}_t given $\mathbf{y}_{1:t-1}$.

Now the maximum-likelihood based semi-supervised learning problem is

$$\begin{aligned}
 \boldsymbol{\theta}^* &= \arg \max_{\boldsymbol{\theta}} \log p(\mathcal{D}_{\text{semi}}; \boldsymbol{\theta}) \\
 &= \arg \max_{\boldsymbol{\theta}} \log p(\{\mathcal{D}_s, \mathcal{D}_u\}; \boldsymbol{\theta}) \\
 &= \arg \max_{\boldsymbol{\theta}} \{\log p(\mathcal{D}_s; \boldsymbol{\theta}) + \log p(\mathcal{D}_u; \boldsymbol{\theta})\}.
 \end{aligned} \tag{14}$$

Then, we can further expand

$$\begin{aligned} \log p(\mathcal{D}_s; \boldsymbol{\theta}) &= \log \prod_{j \in \mathcal{I}_s} p(\mathbf{x}_{1:T^{(j)}}^{(j)}, \mathbf{y}_{1:T^{(j)}}^{(j)}; \boldsymbol{\theta}) \\ &= \log \prod_{j \in \mathcal{I}_s} p(\mathbf{x}_{1:T^{(j)}}^{(j)} | \mathbf{y}_{1:T^{(j)}}^{(j)}; \boldsymbol{\theta}) p(\mathbf{y}_{1:T^{(j)}}^{(j)}; \boldsymbol{\theta}), \end{aligned} \quad (15)$$

and

$$\log p(\mathcal{D}_u; \boldsymbol{\theta}) = \log \prod_{i \in \mathcal{I}_u} p(\mathbf{y}_{1:T^{(i)}}^{(i)}; \boldsymbol{\theta}) \quad (16)$$

Substituting (11), (12), (6), (15), (16) in (14), and converting the logarithm of products to sums, we have the final expression of the semi-supervised learning for SemiDANSE as follows:

$$\begin{aligned} \boldsymbol{\theta}^* &= \arg \max_{\boldsymbol{\theta}} \left\{ \sum_{j \in \mathcal{I}_s} \sum_{t=1}^{T^{(j)}} \log p(\mathbf{x}_t^{(j)} | \mathbf{y}_{1:t}^{(j)}; \boldsymbol{\theta}) \right. \\ &\quad \left. + \sum_{i \in \mathcal{I}_s \cup \mathcal{I}_u} \sum_{t=1}^{T^{(i)}} \log p(\mathbf{y}_{1:t}^{(i)}; \boldsymbol{\theta}) \right\} \\ &= \arg \min_{\boldsymbol{\theta}} \left\{ \sum_{j \in \mathcal{I}_s} \mathcal{L}_s(\mathbf{x}_{1:T^{(j)}}^{(j)}, \mathbf{y}_{1:T^{(j)}}^{(j)}; \boldsymbol{\theta}) \right. \\ &\quad \left. + \sum_{i=1}^N \mathcal{L}_u(\mathbf{y}_{1:T^{(i)}}^{(i)}; \boldsymbol{\theta}) \right\}. \quad (17) \\ &= \arg \min_{\boldsymbol{\theta}} \mathcal{L}(\mathcal{D}_{\text{semi}}; \boldsymbol{\theta}). \end{aligned}$$

In the above expression, the loss term $\mathcal{L}_u(\cdot; \boldsymbol{\theta})$ denotes the loss term due to unsupervised learning, and the $\mathcal{L}_s(\cdot, \cdot; \boldsymbol{\theta})$ is the loss term due to supervised learning. They together can be seen as a total loss $\mathcal{L}(\cdot; \boldsymbol{\theta})$ s.t.

$$\begin{aligned} \mathcal{L}(\mathcal{D}_{\text{semi}}; \boldsymbol{\theta}) &= \sum_{j \in \mathcal{I}_s} \mathcal{L}_s(\mathbf{x}_{1:T^{(j)}}^{(j)}, \mathbf{y}_{1:T^{(j)}}^{(j)}; \boldsymbol{\theta}) \\ &\quad + \sum_{i=1}^N \mathcal{L}_u(\mathbf{y}_{1:T^{(i)}}^{(i)}; \boldsymbol{\theta}) \end{aligned} \quad (18)$$

We note that in the absence of $\mathcal{L}_s(\cdot, \cdot; \boldsymbol{\theta})$, the total loss is only due to unsupervised learning, which is indeed the case for DANSE [16]. We can further expand \mathcal{L}_s as

$$\begin{aligned} \mathcal{L}_s(\mathbf{x}_{1:T^{(j)}}^{(j)}, \mathbf{y}_{1:T^{(j)}}^{(j)}; \boldsymbol{\theta}) &\triangleq - \sum_{t=1}^{T^{(j)}} \log p(\mathbf{x}_t^{(j)} | \mathbf{y}_{1:t}^{(j)}; \boldsymbol{\theta}) \\ &= \sum_{t=1}^{T^{(j)}} \left\{ \frac{m}{2} \log 2\pi + \frac{1}{2} \log \det(\mathbf{L}_{t|1:t}^{(j)}(\boldsymbol{\theta})) \right. \\ &\quad \left. + \frac{1}{2} \|\mathbf{x}_t^{(j)} - \mathbf{m}_{t|1:t}^{(j)}(\boldsymbol{\theta})\|_{(\mathbf{L}_{t|1:t}^{(j)}(\boldsymbol{\theta}))^{-1}}^2 \right\}, \end{aligned} \quad (19)$$

where $\mathbf{m}_{t|1:t}$ and $\mathbf{L}_{t|1:t}$ are computed using (3), (4). Similarly, we can expand \mathcal{L}_u as follows

$$\begin{aligned} \mathcal{L}_u(\mathbf{y}_{1:T^{(i)}}^{(i)}; \boldsymbol{\theta}) &\triangleq - \sum_{t=1}^{T^{(i)}} \log p(\mathbf{y}_t^{(i)} | \mathbf{y}_{1:t-1}^{(i)}; \boldsymbol{\theta}) \\ &= \sum_{t=1}^{T^{(i)}} \left\{ \frac{n}{2} \log 2\pi + \frac{1}{2} \log \det(\mathbf{C}_w + \mathbf{H}\mathbf{L}_{t|1:t-1}^{(i)}(\boldsymbol{\theta})\mathbf{H}^\top) \right. \\ &\quad \left. + \frac{1}{2} \|\mathbf{y}_t^{(i)} - \mathbf{H}\mathbf{m}_{t|1:t-1}^{(i)}(\boldsymbol{\theta})\|_{(\mathbf{C}_w + \mathbf{H}\mathbf{L}_{t|1:t-1}^{(i)}(\boldsymbol{\theta})\mathbf{H}^\top)^{-1}}^2 \right\}. \end{aligned} \quad (20)$$

The overall optimization problem (17) is non-convex and we solve this using gradient descent.

From (17), note that the semi-supervised learning for SemiDANSE translates to the unsupervised learning of DANSE with maximum amount of unlabelled data, when $\mathcal{D}_s = \emptyset$, that means $|\mathcal{I}_u| \triangleq N_u = N$. A small $N_s \triangleq |\mathcal{I}_s| \ll N$ with $\mathcal{D}_s \neq \emptyset$ is intended and interesting for semi-supervised learning.

C. On unsupervised and semi-supervised learning for BSCM

Let us investigate the unsupervised learning of DANSE and why it fails for the BSCM problem. The unsupervised learning problem is as follows.

$$\boldsymbol{\theta}^* = \arg \min_{\boldsymbol{\theta}} \sum_{i=1}^N \mathcal{L}_u(\mathbf{y}_{1:T^{(i)}}^{(i)}; \boldsymbol{\theta}), \quad (21)$$

where \mathcal{L}_u is shown in (20). A natural question is why the learning problem does not work properly for the BSCM problem? Note an important issue when $n < m$: learning of the parameter $\boldsymbol{\theta}$ may not be an underdetermined problem, but the state estimation problem is underdetermined. The supporting argument is in the next paragraph.

Let the total number of scalars in $\boldsymbol{\theta}$ is N_θ . Assuming $T^{(i)} = T, \forall i \in [N]$, the total number of constraints in the unsupervised learning is nNT . Typically $N_\theta < nNT$, and even it can be $N_\theta \ll nNT$, and hence the learning of $\boldsymbol{\theta}$ may not be necessarily underdetermined. However, learning an appropriate $\boldsymbol{\theta}$ for state estimation remains as an underdetermined problem. We can learn $\boldsymbol{\theta}$, and the RNN provides a set of parameters for the Gaussian prior that is consistent with the measurement / observation system, but that does not mean that the learned parameters are consistent with the underlying true states. This not only will lead to a poor Bayesian state estimation performance for the training data, but also for test data. Overall, this phenomenon can be explained conceptually as a limitation of the unsupervised learning because we do not have access to any labelled data for an efficient ‘inductive learning’ that happens in semi-supervised learning [33, Chap. 1].

For semi-supervised learning the total number of constraints is $mN_sT + nNT$ in the optimization problem (17). The mN_sT constraints are related to the use of labelled data amount. This we refer to as a form of ‘supervised regularization’. Recall that typically $N_s \ll N$, and hence a natural question arises: What is the reasonable amount of labelled data, that means the value of N_s compared to N ? In our later experiments, we used $N_s = 2\%$ of N .

However, at this point, we the authors do not have a good argument, preferably a theoretically sound argument, that there can not be any unsupervised learning algorithm for the BSCM problem. In this regard, there can be many questions, for which we have limited answers so far. Some example questions are as follows.

- 1) Can the unsupervised learning will work if N increases? That means when we have a lot of unlabelled data.
- 2) What can be the interplay between n , m , N and the complexity of the underlying nonlinear process $\{\mathbf{x}_t\}$?

III. EXPERIMENTS AND RESULTS

In this section, we perform experiments using complex nonlinear processes for which we generate data knowing their SSMs. While SemiDANSE does not the know the SSMs during learning or inference, the model-based methods know the SSMs. We discuss the following: (1) three chaotic dynamical systems that we simulate as the nonlinear processes; (2) information about training and testing, performance measures and RNN; (3) competing Bayesian state estimation methods; and finally (4) experiments for BSCM problem.

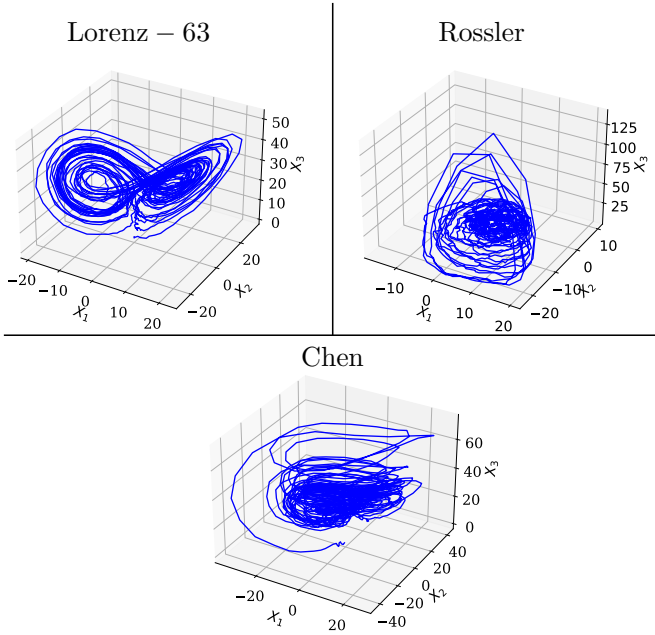


Fig. 3: Visualization of three chaotic dynamical systems: randomly chosen state trajectories from the test set of length $T_{\text{test}} = 2000$ for the Lorenz-63, Chen, and Rössler attractors. The state trajectories show variations of the three systems.

A. Three chaotic dynamical systems

In this subsection, we briefly describe three chaotic dynamical systems used for experiments as benchmark nonlinear systems. They are

- 1) The Lorenz-63 attractor [18],
- 2) The Chen attractor [20], and
- 3) The Rössler attractor [21].

These three systems are 3-dimensional with highly complex state dynamics. We simulate each of the chaotic dynamical systems by discretizing their original continuous-time dynamics following [16] and incorporate i.i.d. process noise to ensure randomness. The detailed equations for their state dynamics (or SSM) and simulation procedures are described in Appendix B. All of them are Markovian processes. Appropriate process noise is incorporated in Markovian state transition such that the chaotic dynamical systems are not deterministic, but random in statistical nature. For visualization, we show randomly chosen test set trajectories of the three processes in Fig. 3. This figure helps to visualize how different the trajectories can be across the three chaotic dynamical systems, and a qualitative justification for use of them in state estimation experiments across different dynamical systems.

B. Training, testing, performance measures and RNN

We have training datasets as described in subsection II-B for DANSE, DMM and SemiDANSE, and a testing dataset $\mathcal{D}_{\text{test}} = \left\{ \left(\mathbf{x}_{1:T_{\text{test}}^{(j)}}^{(j)}, \mathbf{y}_{1:T_{\text{test}}^{(j)}}^{(j)} \right) \right\}_{j=1}^{N_{\text{test}}}$. We mention that SemiDANSE is trained using $\mathcal{D}_{\text{semi}}$, thus involving a combination of labelled and unlabelled data. For training, we use a dataset where

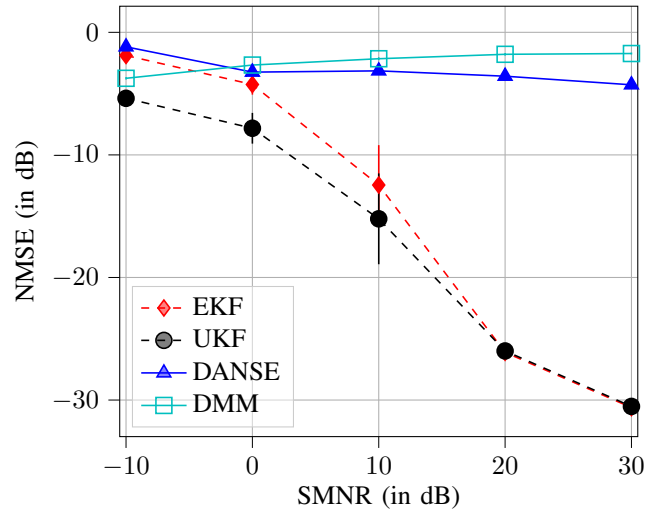


Fig. 4: The average NMSE (in dB) on $\mathcal{D}_{\text{test}}$ versus SMNR (in dB) performances to illustrate failure of unsupervised learning-based data-driven DANSE and DMM for the BSCM problem setup described in subsection III-D. The model-driven EKF and UKF perform well.

$N = 1000$ (total number of training trajectories) and having the same length $T = 100$ for each training trajectory. For testing, we use a dataset $\mathcal{D}_{\text{test}}$ where $N_{\text{test}} = 100$ (total number of testing trajectories) and having the same length $T_{\text{test}} = 2000$ for each testing trajectory. Denoting the estimated state as $\hat{\mathbf{x}}_t$ (for example the posterior mean), we use the averaged normalized-mean-squared-error (NMSE) in decibels (dB) as the performance measure, defined below as in [16, section III].

$$\text{NMSE} = \frac{1}{N_{\text{test}}} \sum_{j=1}^{N_{\text{test}}} 10 \log_{10} \frac{\sum_{t=1}^{T_{\text{test}}^{(j)}} \|\mathbf{x}_t^{(j)} - \hat{\mathbf{x}}_t^{(j)}\|_2^2}{\sum_{t=1}^{T_{\text{test}}^{(j)}} \|\mathbf{x}_t^{(j)}\|_2^2}. \quad (22)$$

For experiments we use iid Gaussian noise as the measurement noise, the means $\mathbf{C}_w = \sigma_w^2 \mathbf{I}_n$. The signal-to-measurement noise ratio (SMNR) is calculated in dB, same as in [16, section III] on $\mathcal{D}_{\text{test}}$, as

$$\begin{aligned} \text{SMNR} &= \frac{1}{N_{\text{test}}} \sum_{j=1}^{N_{\text{test}}} 10 \log_{10} \left(\frac{\sum_{t=1}^{T_{\text{test}}^{(j)}} \mathbb{E} \{ \|\mathbf{H}\mathbf{x}_t^{(j)} - \mathbb{E} \{ \mathbf{H}\mathbf{x}_t^{(j)} \} \|_2^2 \}}{\text{tr}(\mathbf{C}_w)} \right) \\ &= \frac{1}{N_{\text{test}}} \sum_{j=1}^{N_{\text{test}}} 10 \log_{10} \left(\frac{\sum_{t=1}^{T_{\text{test}}^{(j)}} \mathbb{E} \{ \|\mathbf{H}\mathbf{x}_t^{(j)} - \mathbb{E} \{ \mathbf{H}\mathbf{x}_t^{(j)} \} \|_2^2 \}}{n\sigma_w^2} \right). \end{aligned} \quad (23)$$

For notational convenience, we also introduce a parameter

$$\kappa \triangleq \frac{N_s}{N}, \quad 0 \leq \kappa \leq 1. \quad (24)$$

The parameter κ provides a measure to quantify the relative amount of labelled data and unlabelled data in semi-supervised learning. As a concrete example, we used $N = 1000$ $N_s = 20$ for all our experiments later. That means $\kappa = 0.02 = 2\%$, and SemiDANSE uses 2% labelled data along-with the total amount of unlabelled data. Further, the semi-supervised learning in subsection II-B is formulated in a way that when $\kappa = 0$ then the semi-supervised learning translates to unsupervised

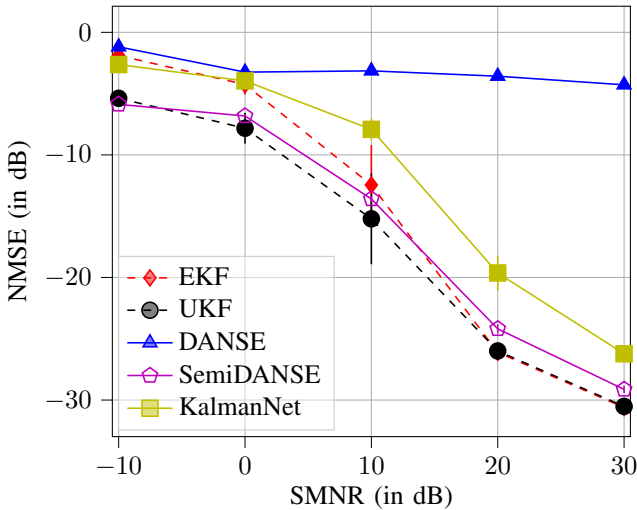


Fig. 5: The average NMSE (in dB) on $\mathcal{D}_{\text{test}}$ versus SMNR (in dB) performances to illustrate success of SemiDANSE for the BSCM problem setup described in subsection III-D. The SemiDANSE ($\kappa = 0.02$) is compared with the model-driven EKF and UKF, the hybrid KalmanNet [17] and the unsupervised learning-based data-driven DANSE.

learning. That means, SemiDANSE translates to DANSE when $\kappa = 0$.

1) *RNN architecture*: We found the RNN architecture that includes appropriate feed-forward networks by cross-validation. For SemiDANSE, we experimented with both LSTM and GRU and found the suitable RNN architecture to be a GRU [36], [38]. The GRU has 1 hidden layer with 30 hidden nodes. The output of the RNN is passed to shallow feed-forward networks FC_m, FC_L as described in Fig. 2 for calculating the means and the covariances. The feed-forward networks have 2 hidden layers, where the first hidden layer has 30 hidden nodes and shared between FC_m and FC_L . The output layer was designed to have 32 hidden nodes and distinct for FC_m and FC_L . The mathematical details of the feed-forward networks are described in (29) in Appendix A. We implemented SemiDANSE in Python and PyTorch [39] and trained the architecture using a single NVIDIA Tesla P100 GPU card¹. The training algorithm uses a mini-batch gradient descent with a batch size of 64. The optimizer chosen was Adam [40] with an adaptive learning rate set at a starting value 5×10^{-4} and decreased by 10% every $1/6^{\text{th}}$ of the maximum number of training epochs. The maximum number of training epochs was set at 2000, and an early stopping criterion based on the MSE of the validation set was used to avoid overfitting similar to DANSE.

C. Competing methods

In this subsection, we compare SemiDANSE vis-à-vis a few other Bayesian state estimation methods like [16] on the BSCM task. The methods that we compare are:

- 1) model-based EKF and UKF,

- 2) data-driven causal DMM and DANSE,
- 3) hybrid method KalmanNet.

The model-based EKF and UKF have full knowledge of the SSM of underlying process. They are implemented using Python, PyTorch and FilterPy [41]. The DMM and DANSE methods are implemented in PyTorch and trained by unsupervised learning that uses \mathcal{D}_u . DMM assumes that the underlying process is Markovian, but it does not know the SSM of the process. A brief description of the learning problem for the DMM that we implemented in this article is given in Appendix C. DANSE does not have any knowledge of the underlying process. The KalmanNet is trained by unsupervised learning that uses \mathcal{D}_u and it also has the full knowledge of the SSM of underlying process. All these competing methods, their training and simulations are described in [16, section III], and hence we restrain for further discussion about them.

D. Failure of unsupervised DANSE and DMM for BSCM

We begin our experiments with Lorenz-63 system where we first show failure of unsupervised learning-based methods - DANSE and DMM. For the experiment we use 2×3 -dimensional \mathbf{H} matrix where each element is drawn from i.i.d. Gaussian source $\mathcal{N}(0, 1)$ and then fixed. Therefore we have $n = 2$ and $m = 3$, and the \mathbf{H} matrix we use for the BSCM problem is

$$\mathbf{H} = \begin{bmatrix} 0.37992 & 0.34099 & 1.04317 \\ 0.98070 & -0.70477 & 2.17908 \end{bmatrix}. \quad (25)$$

In Fig. 4 we show the NMSE versus SMNR performances of DANSE and DMM, and only include the performances of EKF and UKF for comparison. We note that both DANSE and DMM were trained on different SMNRs as shown in Fig. 4 and tested on the same SMNRs. It shows that the model-driven EKF and UKF performs well, but the unsupervised learning-based data-driven DANSE and DMM - both of them - fail to perform. Note that the Lorenz-63 system that we simulated is a Markovian process and DMM uses the knowledge that the underlying process is Markovian, but still that knowledge is not good enough to address the BSCM problem.

Here, for completeness, we mention that if the \mathbf{H} matrix would be a full column-rank matrix, for example a 3×3 -dimensional full rank matrix, then DANSE and DMM could perform well. This can be checked from [16, section III-D]. For brevity we do not show the performance for such full column-rank \mathbf{H} matrix because that is not the BSCM problem.

E. Success of SemiDANSE for BSCM

For the same setup of the previous subsection III-D we now show the performance of SemiDANSE and compare it with EKF, UKF and KalmanNet in Fig. 5. As in subsection III-D, SemiDANSE was also trained and tested on different SMNRs using $\kappa = 0.02$ to keep the comparison consistent. We observe that SemiDANSE is competitive. It overcomes the limitation of DANSE for the BSCM problem. Note that the use of 2% labelled data regularizes the learning of RNN in SemiDANSE and it delivers a good performance.

¹The code will be made available upon request.

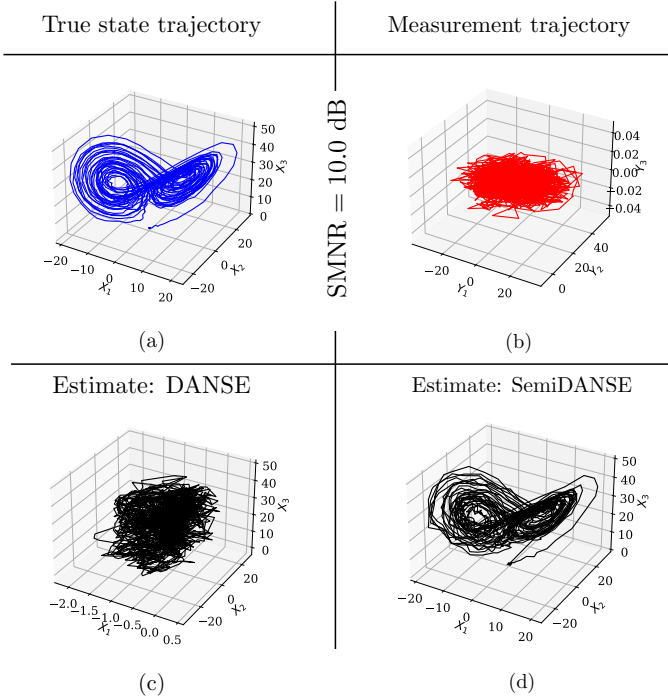


Fig. 6: Demonstrating failure of DANSE and success of SemiDANSE for BSCM problem with partial measurement of Lorenz-63 process. We use the BSCM problem setup described in subsection III-F, where \mathbf{H} is shown in (26), SMNR = 10 dB and σ_e^2 corresponding to -10 dB. (a) A 3-dimensional true state trajectory instance of Lorenz-63 system from $\mathcal{D}_{\text{test}}$. (b) The corresponding 2-dimensional (noisy) measurement trajectory (shown in three-dimension for visualization). (c) The estimate of DANSE (posterior mean). (d) The estimate of SemiDANSE (posterior mean) with $\kappa = 0.02$.

F. Partial measurement system

In the previous two subsections, we had a dense \mathbf{H} matrix providing the 2-dimensional measurement vector \mathbf{y}_t that has influences from all the three components of the state vector \mathbf{x}_t . Instead of a dense \mathbf{H} , we can have scenarios where only some components of the state vectors are measured (observed). We refer to these scenarios as partial measurement scenarios.

Let us assume that that a partial measurement matrix is

$$\mathbf{H} = \begin{bmatrix} 0 & 1 & 0 \\ 0 & 0 & 1 \end{bmatrix}. \quad (26)$$

That means we have measurements from the second and third components of the 3-dimensional state vector. Fig. 6 shows a 3-dimensional trajectory of the Lorenz-63 process, its 2-dimensional measurement at SMNR = 10 dB, the estimated trajectory using DANSE, and the same using SemiDANSE. It is clear that DANSE fails for the BSCM problem and SemiDANSE performs well.

In Fig. 7 we show the time trajectory of the first component $x_{t,1}$ of \mathbf{x}_t , and estimates of UKF, DANSE and SemiDANSE. DANSE fails to track $x_{t,1}$, and we observe that the model-driven UKF and the data-driven SemiDANSE perform well.

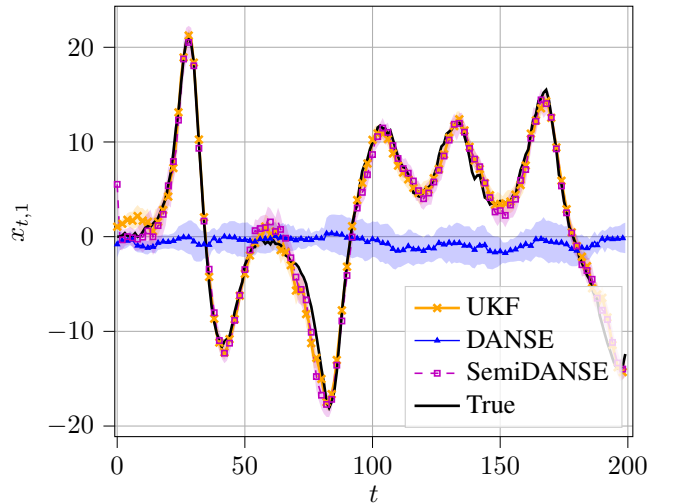


Fig. 7: Time-wise plot of a (true) state trajectory $x_{t,1}$ from $\mathcal{D}_{\text{test}}$ and its estimates using UKF, DANSE and SemiDANSE ($\kappa = 0.02$) at SMNR = 10 dB and σ_e^2 corresponding to -10 dB for the Lorenz-63 process. The results are for the BSCM problem setup described in subsection III-F. The solid / dashed line represents corresponding posterior mean estimate. The shaded region in each of the plots represents the $\pm 1\sigma$ point uncertainty around the corresponding posterior mean estimate. Note that DANSE fails to track the true state, but UKF and SemiDANSE could track. A short portion of the test trajectory is shown for ease of visualization.

Note that the 2-dimensional measurement \mathbf{y}_t has observations of $x_{t,2}$ and $x_{t,3}$ under noise. From our experiments we have seen that while DANSE fails to estimate $x_{t,1}$, it is able to estimate $x_{t,2}$ and $x_{t,3}$. We do not show the plots of the estimates of $x_{t,2}$ and $x_{t,3}$ for brevity. On the other hand, SemiDANSE could track all the three components of \mathbf{x}_t .

G. On predictive performance / forecasting

In this subsection, we show that DANSE provides a good predictive / forecasting performance for tracking the measurement sequence \mathbf{y}_t despite failing to estimate the underlying state sequence \mathbf{x}_t , that means failing to address the BSCM for the partial measurement system in subsection III-F. In Fig. 8, we plot the time-wise and coordinate-wise values of the measurement vector \mathbf{y}_t and the corresponding one-step ahead predicted measurement $\hat{\mathbf{y}}_t$ given $\mathbf{y}_{1:t-1}$ using DANSE and SemiDANSE at 10 dB SMNR for the Lorenz-63 process. Here $\hat{\mathbf{y}}_t$ is the predictive mean of $p(\mathbf{y}_t | \mathbf{y}_{1:t-1})$ (see (13) for SemiDANSE.). A notable fact is that DANSE provides reasonably good predictive performance compared the proposed SemiDANSE, which shows that the DANSE is able to capture the underlying dynamics of the measurements, but the structure of \mathbf{H} in (26) renders it difficult to track the unobserved state vector coordinate $x_{t,1}$ as shown in Fig. 7.

This result for DANSE concludes a fact: unsupervised learning may provide a good predictive / forecasting performance on measurement data as a consequence of efficient time-series modelling, but that may not translate to a good state estimation

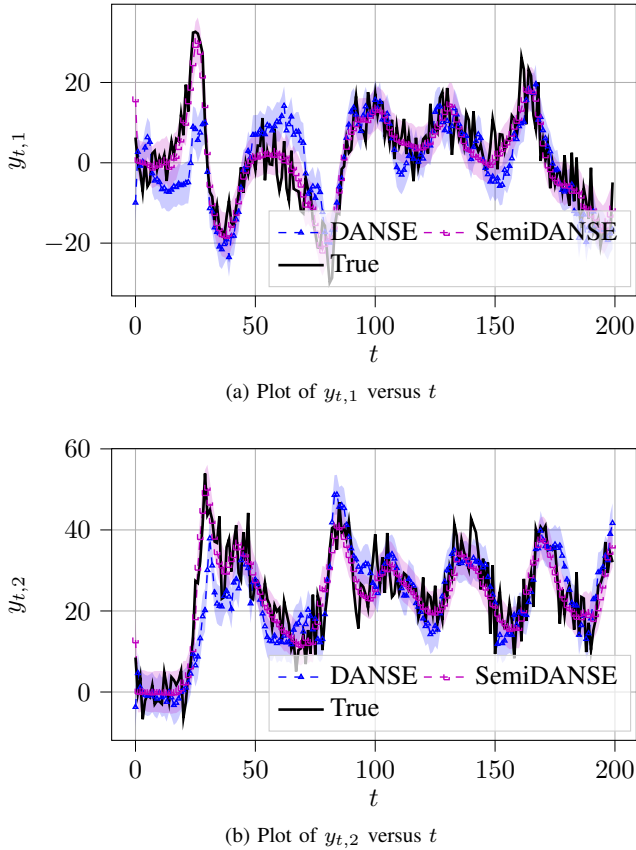


Fig. 8: Time-wise plots of the coordinates of \mathbf{y}_t from $\mathcal{D}_{\text{test}}$ and the one-step ahead predicted estimates using DANSE and SemiDANSE ($\kappa = 0.02$) at SMNR = 10 dB and σ_e^2 corresponding to -10 dB. The results are related to the partial measurement system described in subsections III-F, III-G and for the Lorenz-63 process. The shaded region in each plot shows the $\pm 1\sigma$ point uncertainty of the corresponding predicted estimated of $\{\mathbf{y}_t\}$.

performance. Estimating the hidden state from measurements proves to be a harder task than modeling measurement time-series data.

H. Partial measurement scenario - an extreme BSCM case

In the previous subsection we had measurements from two components of the three dimensional state vector of the Lorenz-63 process. An extreme BSCM problem case is: we have only measurement from one state component. For example, we have the following measurement matrix

$$\mathbf{H} = \begin{bmatrix} 1 & 0 & 0 \end{bmatrix}. \quad (27)$$

That means we have the measurement of the first component of the 3-dimensional state vector. In this extreme case, Fig. 9 shows a 3-dimensional trajectory of the Lorenz-63 process, and the 3-dimensional state estimates from DANSE, UKF and SemiDANSE at SMNR = 10 dB. We observe again that data-driven SemiDANSE and model-driven UKF perform well, but unsupervised learning-based DANSE fails.

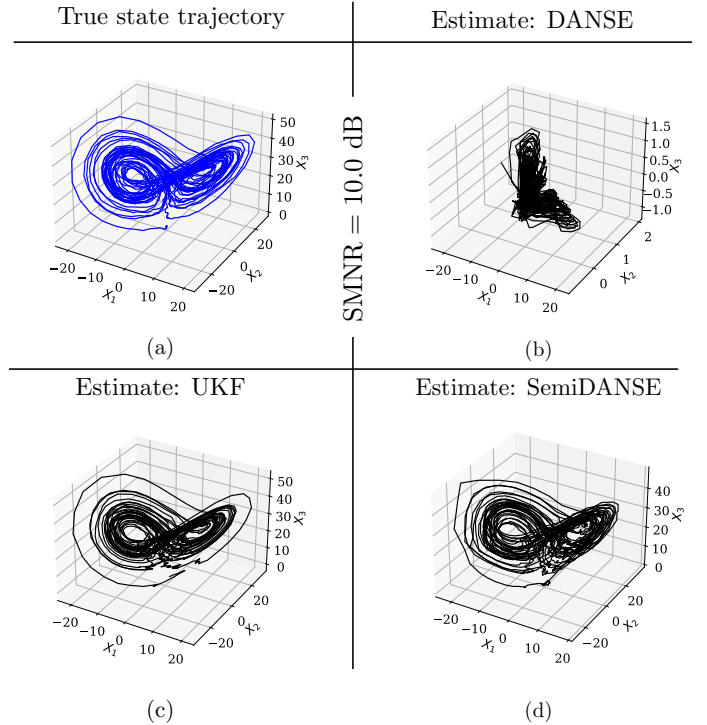


Fig. 9: Demonstrating failure of DANSE and success of SemiDANSE for the extreme BSCM problem with one-dimensional partial measurement of 3-dimensional Lorenz-63 process. We use the BSCM problem setup described in subsection III-H, where the 1×3 measurement matrix \mathbf{H} is shown in (27), SMNR = 10 dB and σ_e^2 corresponding to -10 dB. A 3-dimensional true state trajectory from $\mathcal{D}_{\text{test}}$ is shown in (a). The estimates for DANSE, UKF and SemiDANSE ($\kappa = 0.02$) are all posterior mean estimates shown in (b), (c) and (d) respectively.

I. Demonstration for two more chaotic dynamical systems

As a final experiment, we also show the performance of SemiDANSE on two other chaotic dynamical systems - the Chen attractor and the Rössler attractor - for partial measurement setups. We use the 2×3 -dimensional \mathbf{H} matrix shown in (26) and SMNR = 10 dB. From Fig. 10 and Fig. 11 we observe that while DANSE fails, SemiDANSE succeeds.

IV. CONCLUSIONS

In this article we introduce the BSCM problem for model-free process. We first show that unsupervised learning has limitation to address the BSCM problem using two data-driven state estimation methods - DANSE and DMM. DMM uses a-priori knowledge that the underlying process is Markovian, but that does not help for the BSCM problem. We also find that the unsupervised learning-based DANSE provides a good predictive / forecasting performance to track the measurement data (as a time-series modelling task), but fails to provide a good state estimation performance (estimating the hidden variable from observations). Then we develop a semi-supervised learning-based DANSE method referred to as SemiDANSE and find that it succeeds to address the BSCM problem. We

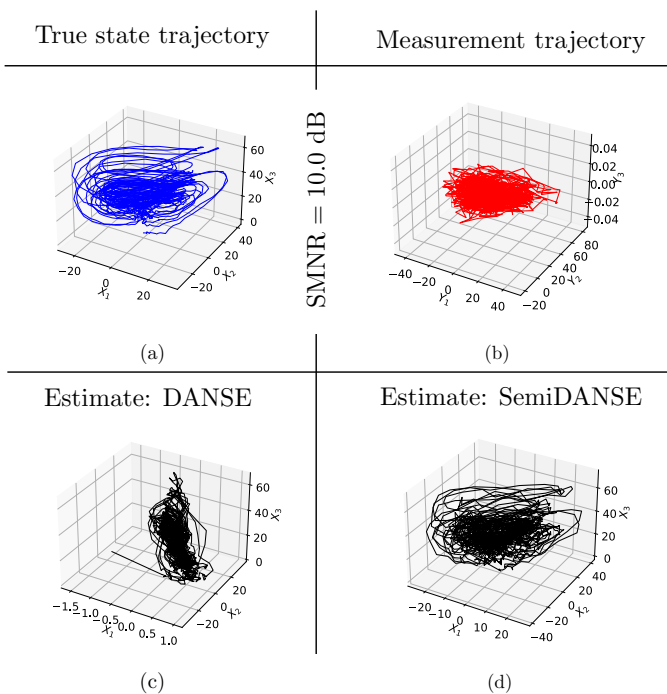


Fig. 10: Additional example of the failure of DANSE and success of SemiDANSE for BSCM problem with partial measurement of 3-dimensional Chen process. We use the 2×3 measurement matrix \mathbf{H} shown in (26). A 3-dimensional true state trajectory from $\mathcal{D}_{\text{test}}$ with σ_e^2 corresponding to -10 dB is shown in (a). The corresponding measurement trajectory at $\text{SMNR} = 10$ dB is shown in (b). The estimates for DANSE and SemiDANSE ($\kappa = 0.02$) are posterior mean estimates shown in (c) and (d) respectively.

show that the use of a limited amount of labelled data, such as 2% of the full training data comprised of labelled and unlabelled data, shows remarkable improvement in learning, leading to desired regularization and a good state estimation performance. Our results reinforces the power of semi-supervised learning in the general field of signal processing and machine learning.

APPENDIX

A. Parameterization of the Gaussian prior using RNN

In this subsection, we describe the parameterization of the Gaussian prior using RNN in (2). The schematic representation for the same is shown in Fig. 2. From Fig. 2 we can see that the prior parameters $\mathbf{m}_{t|1:t-1}$ and $\mathbf{L}_{t|1:t-1}$ are calculated using an RNN together with feed-forward networks using $\mathbf{y}_{1:t-1}$ as input.

Let the internal state of the RNN at time τ be $\mathbf{z}_\tau \in \mathbb{R}^p$. For a causal system, we use unidirectional RNNs, where \mathbf{z}_τ generally depends on the *previous* internal state $\mathbf{z}_{\tau-1}$ and the current input \mathbf{y}_τ as

$$\mathbf{z}_\tau = \varphi(\mathbf{W}_{zz}\mathbf{z}_{\tau-1} + \mathbf{b}_{zz} + \mathbf{W}_{zy}\mathbf{y}_\tau + \mathbf{b}_{zy}), \quad (28)$$

where $\mathbf{W}_{zz} \in \mathbb{R}^{p \times p}$, $\mathbf{b}_{zz} \in \mathbb{R}^{p \times 1}$, $\mathbf{W}_{zy} \in \mathbb{R}^{p \times m}$, $\mathbf{b}_{zy} \in \mathbb{R}^{p \times 1}$ denote the learnable weights and biases for the connections between the hidden states and the inputs, $\varphi(\cdot)$

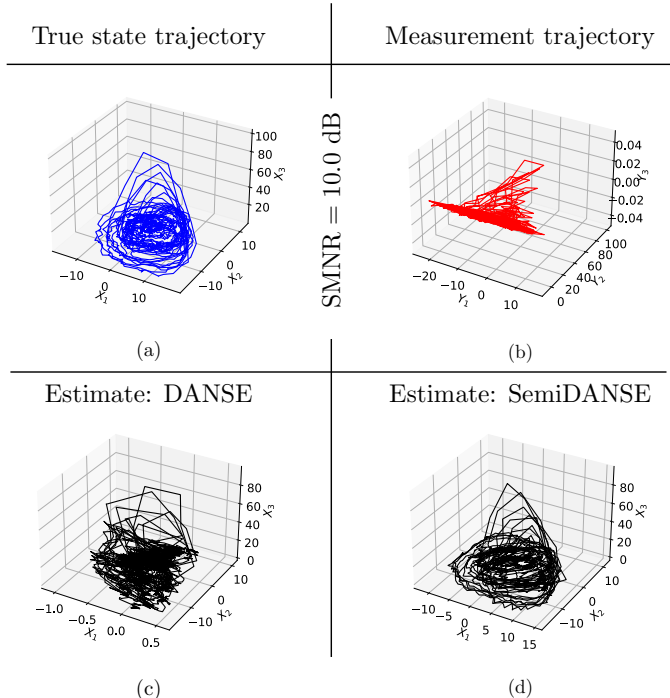


Fig. 11: Additional example of the failure of DANSE and success of SemiDANSE for BSCM problem with partial measurement of 3-dimensional Rössler process. We use the 2×3 measurement matrix \mathbf{H} shown in (26). A 3-dimensional true state trajectory from $\mathcal{D}_{\text{test}}$ with σ_e^2 corresponding to -15 dB is shown in (a). The corresponding measurement trajectory at $\text{SMNR} = 10$ dB is shown in (b). The estimates for DANSE and SemiDANSE ($\kappa = 0.02$) are posterior mean estimates shown in (c) and (d) respectively.

denotes a nonlinear function [42, Chap. 10]. For the simplest RNN architectures such as a vanilla RNN, $\varphi(\cdot)$ can be as simple as an element-wise activation like a hyperbolic tangent function ($\tanh(\cdot)$) or can be much more complicated for sophisticated architectures such as GRUs and LSTMs involving gating functions [36], [38]. In our case, $\varphi(\cdot)$ is the nonlinear function for a GRU [36]. The parameters of the RNN $\mathbf{W}_{zz}, \mathbf{b}_{zz}, \mathbf{W}_{zy}, \mathbf{b}_{zy}$ are shared across time and learning happens in accordance with backpropagation through time (BPTT) [43]. The internal state at the $(t-1)$ 'th time instant \mathbf{z}_{t-1} captures the information of the sequence $\mathbf{y}_{1:t-1}$. We then map \mathbf{z}_{t-1} to the mean $\mathbf{m}_{t|1:t-1}$ and the covariance $\mathbf{L}_{t|1:t-1}$ using two shallow feed-forward networks FC_m, FC_L through an intermediate representation \mathbf{z}'_{t-1} as follows

$$\begin{aligned} \mathbf{z}'_{t-1} &= \text{ReLU}(\mathbf{W}_{z'z}\mathbf{z}_{t-1} + \mathbf{b}_{z'z}), \\ \mathbf{m}_{t|1:t-1} &= \text{FC}_m(\mathbf{z}'_{t-1}) \\ &= \mathbf{W}_{mz'}\mathbf{z}'_{t-1} + \mathbf{b}_{mz'}, \\ \mathbf{L}_{t|1:t-1} &= \text{diag}(\text{FC}_L(\mathbf{z}'_{t-1})) \\ &= \text{diag}\left(\text{softplus}\left(\mathbf{W}_{Lz'}\mathbf{z}'_{t-1} + \mathbf{b}_{Lz'}\right)\right), \end{aligned} \quad (29)$$

where $\mathbf{W}_{mz'} \in \mathbb{R}^{m \times p'}$, $\mathbf{b}_{mz'} \in \mathbb{R}^{m \times 1}$, $\mathbf{W}_{Lz'} \in \mathbb{R}^{m \times p'}$, $\mathbf{b}_{Lz'} \in \mathbb{R}^{m \times 1}$, $\mathbf{W}_{z'z} \in \mathbb{R}^{p' \times p}$, $\mathbf{b}_{z'z} \in \mathbb{R}^{p' \times 1}$ are learnable weights and biases, $\text{ReLU}(x) = \max(0, x)$ is the element-wise, rectified linear unit function and

$\text{softplus}(x) = \log(1 + \exp(x))$ is the element-wise, smooth approximation to $\text{ReLU}(x)$ [39]. As explained in section II-A, $\mathbf{L}_{t|1:t-1}$ is modelled as a diagonal covariance matrix in accordance with (29). Thus, as per the notation in (2), the full set of learnable parameters is $\theta = \{\mathbf{W}_{zz}, \mathbf{b}_{zz}, \mathbf{W}_{zy}, \mathbf{b}_{zy}, \mathbf{W}_{mz'}, \mathbf{b}_{mz'}, \mathbf{W}_{Lz'}, \mathbf{b}_{Lz'}, \mathbf{W}_{z'z}, \mathbf{b}_{z'z}\}$. The specific architectures of the RNN and the feed-forward networks are chosen by grid-search and described in section III-B.

B. Three chaotic dynamical systems

In this subsection, we briefly describe the mathematical models of the three chaotic dynamical systems used for experiments in section III-A. The first two chaotic dynamical systems - the Lorenz-63 attractor [18] and the Chen attractor [20] were developed independently but have been shown to be belonging to possess a generalized Lorenz canonical form in [19]. We used the discretized form of the Lorenz-63 attractor described in [16], as follows:

$$\begin{aligned} \mathbf{x}_{t+1} &= \mathbf{f}_t^{(L)}(\mathbf{x}_t) + \mathbf{e}_t^{(L)} \in \mathbb{R}^3, \\ &= \mathbf{F}_t^{(L)}(\mathbf{x}_t)\mathbf{x}_t + \mathbf{e}_t^{(L)} \in \mathbb{R}^3, \end{aligned} \quad (30)$$

$$\text{s.t. } \mathbf{F}_t^{(L)}(\mathbf{x}_t) = \exp\left(\begin{bmatrix} -10 & 10 & 0 \\ 28 & -1 & -x_{t,1} \\ 0 & x_{t,1} & -\frac{8}{3} \end{bmatrix} \Delta\right),$$

where the process noise $\mathbf{e}_t^{(L)} \sim \mathcal{N}(\mathbf{e}_t^{(L)}; \mathbf{0}, \mathbf{C}_e^{(L)})$ with $\mathbf{C}_e^{(L)} = \sigma_e^2 \mathbf{I}_3$, the step-size $\Delta = 0.02$ seconds. σ_e^2 was set corresponding to -10 dB. The subscript (L) refers to the Lorenz attractor. In our simulations, we use a finite-Taylor series approximation of 5'th order for the matrix exponential in $\mathbf{F}_t^{(L)}(\mathbf{x}_t)$.

The Chen attractor has mathematically a very similar form to the Lorenz-63 attractor except that the constants in the SSM are different. Similar to (30), it has the following mathematical form

$$\mathbf{x}_{t+1} = \mathbf{F}_t^{(C)}(\mathbf{x}_t)\mathbf{x}_t + \mathbf{e}_t^{(C)} \in \mathbb{R}^3, \quad (31)$$

$$\text{s.t. } \mathbf{F}_t^{(C)}(\mathbf{x}_t) = \exp\left(\begin{bmatrix} -35 & 35 & 0 \\ -7 & 28 & -x_{t,1} \\ 0 & x_{t,1} & -3 \end{bmatrix} \Delta'\right),$$

where $\mathbf{e}_t^{(C)} \sim \mathcal{N}(\mathbf{e}_t^{(C)}; \mathbf{0}, \mathbf{C}_e^{(C)})$ with $\mathbf{C}_e^{(C)} = \sigma_e^2 \mathbf{I}_3$, the step-size $\Delta' = 0.002$ seconds. σ_e^2 was set corresponding to -10 dB. In our simulations, we use a finite-Taylor series approximation of 5'th order for the matrix exponential in $\mathbf{F}_t^{(C)}(\mathbf{x}_t)$.

The Rössler attractor [21] appears simpler than the above two in terms of non-linear relationships among the state variables. Similar to (30), (31), it has the following mathematical form

$$\mathbf{x}_{t+1} = \mathbf{F}_t^{(R)}(\mathbf{x}_t)\mathbf{x}_t + \mathbf{e}_t^{(R)} \in \mathbb{R}^3, \quad (32)$$

$$\begin{aligned} \text{s.t. } \mathbf{F}_t^{(R)}(\mathbf{x}_t) \\ = \exp\left(\begin{bmatrix} 0 & -1 & -1 \\ 1 & 0.2 & 0 \\ 0 & 0 & \frac{0.2}{x_{t,3}} + (x_{t,1} - 5.7) \end{bmatrix} \Delta''\right), \end{aligned}$$

$$\text{where } \mathbf{e}_t^{(R)} \sim \mathcal{N}(\mathbf{e}_t^{(R)}; \mathbf{0}, \mathbf{C}_e^{(R)}) \text{ with } \mathbf{C}_e^{(R)} = \begin{bmatrix} \sigma_e^2 & 0 & 0 \\ 0 & \sigma_e^2 & 0 \\ 0 & 0 & \epsilon \end{bmatrix},$$

$\epsilon \in \mathbb{R}_+$ is constant, the step-size $\Delta'' = 0.008$ seconds. In our simulations, we use a finite-Taylor series approximation of 5'th order for the matrix exponential in $\mathbf{F}_t^{(R)}(\mathbf{x}_t)$. For all the three systems, the measurement system is the linear measurement system in (1), with the measurement noise is $\mathbf{w}_t \sim \mathcal{N}(\mathbf{w}_t; \mathbf{0}, \mathbf{C}_w)$ with $\mathbf{C}_w = \sigma_w^2 \mathbf{I}_3$. σ_w^2 was set corresponding to -15 dB. The truncated, reduced process noise variance is used in the simulation of the Rössler attractor in (32) to avoid numerical problems owing to incorporating noise in the dynamics. Since all the systems do not have the same step-size, in order to get a trajectory of length T with a similar degree of captured dynamics as the Lorenz-63 attractor, the other ones viz. Chen and Rössler are simulated for longer T , and then decimated in time by an appropriate factor (depending on the step-size) to get a trajectory of length T .

C. DMM - Learning problem

The deep Markov model (DMM) method proposed in [13] is well-suited to the modeling of complex time-series signals. A detailed description of the different inference modes and training architectures of the DMM can be found in [13], [30, Chap. 5]. Here, we provide a brief description of the DMM that we used for comparison in section III.

The DMM method relies on a choice of an *approximate* posterior distribution $q(\mathbf{x}_{1:T}|\mathbf{y}_{1:T}; \phi)$ parameterized using a deep recurrent neural network with parameters ϕ . The factorization of this approximate posterior defines the inference mode used. For e.g. in this work, we employed the structured left-information (ST-L) mode, as it gives rise to a causal filtering scenario [13]. The approximate posterior would then factorize as

$$q(\mathbf{x}_{1:T}|\mathbf{y}_{1:T}; \phi) = \prod_{t=1}^T q(\mathbf{x}_t|\mathbf{x}_{t-1}\mathbf{y}_{1:t}; \phi). \quad (33)$$

In addition to this, the DMM method assumes that the process state dynamics is Markovian and tries to learn a model $p(\mathbf{x}_t|\mathbf{x}_{t-1}; \psi)$ with learnable parameters ψ . This is achieved by optimizing a variational lower bound (VLB) using (1), (33) and the Markovian assumption as follows:

$$\begin{aligned} &\log p(\mathbf{y}_{1:T}; \psi) \\ &= \log\left(\int \cdots \int p(\mathbf{y}_{1:T}, \mathbf{x}_{1:T}; \psi) d\mathbf{x}_1 \cdots d\mathbf{x}_T\right) \\ &= \log\left(\int \cdots \int q(\mathbf{x}_{1:T}|\mathbf{y}_{1:T}; \phi) \frac{p(\mathbf{y}_{1:T}, \mathbf{x}_{1:T}; \psi)}{q(\mathbf{x}_{1:T}|\mathbf{y}_{1:T}; \phi)} d\mathbf{x}_1 \cdots d\mathbf{x}_T\right) \\ &\stackrel{(a4)}{\geq} \int \cdots \int q(\mathbf{x}_{1:T}|\mathbf{y}_{1:T}; \phi) \log\left(\frac{p(\mathbf{y}_{1:T}, \mathbf{x}_{1:T}; \psi)}{q(\mathbf{x}_{1:T}|\mathbf{y}_{1:T}; \phi)}\right) d\mathbf{x}_1 \cdots d\mathbf{x}_T \\ &= \mathbb{E}_{q(\mathbf{x}_{1:T}|\mathbf{y}_{1:T}; \phi)} \left[\log\left(\frac{p(\mathbf{y}_{1:T}, \mathbf{x}_{1:T}; \psi)}{q(\mathbf{x}_{1:T}|\mathbf{y}_{1:T}; \phi)}\right) \right] \\ &= \mathbb{E}_{q(\mathbf{x}_{1:T}|\mathbf{y}_{1:T}; \phi)} \left[\log p(\mathbf{y}_{1:T}|\mathbf{x}_{1:T}; \psi) \right] \\ &\quad + \mathbb{E}_{q(\mathbf{x}_{1:T}|\mathbf{y}_{1:T}; \phi)} \left[\log\left(\frac{p(\mathbf{x}_{1:T}; \psi)}{q(\mathbf{x}_{1:T}|\mathbf{y}_{1:T}; \phi)}\right) \right] \\ &\stackrel{(b4)}{=} \sum_{t=1}^T \mathbb{E}_{q(\mathbf{x}_t|\mathbf{y}_{1:t}; \phi)} [\log \mathcal{N}(\mathbf{y}_t; \mathbf{H}\mathbf{x}_t, \mathbf{C}_w)] \\ &\quad - \mathbb{E}_{q(\mathbf{x}_{t-1}|\mathbf{y}_{1:t-1}; \phi)} [\text{DKL}(q(\mathbf{x}_t|\mathbf{x}_{t-1}, \mathbf{y}_{1:t}; \phi) \| p(\mathbf{x}_t|\mathbf{x}_{t-1}; \psi))] \\ &\triangleq \mathcal{L}(\psi, \phi; \mathbf{y}_{1:T}), \end{aligned}$$

where the inequality in (a4) is obtained by Jensen’s inequality and the detailed derivation of the equality in (b4) is detailed in [30, Chap. 5]. In practice, we evaluate the above expectations using Monte-Carlo approximations and sequential sampling with the reparameterization trick [44], making it quite computationally expensive. For a training dataset $\mathcal{D} = \{\mathbf{y}_{1:T^{(i)}}^{(i)}\}_{i=1}^N$, the optimization problem then becomes

$$\boldsymbol{\psi}^*, \boldsymbol{\phi}^* = \arg \max_{\boldsymbol{\psi}, \boldsymbol{\phi}} \sum_{i=1}^N \mathcal{L}(\boldsymbol{\psi}, \boldsymbol{\phi}; \mathbf{y}_{1:T^{(i)}}^{(i)}). \quad (34)$$

The inference follows by sequentially sampling from the learned, approximate posterior $q(\mathbf{x}_t | \mathbf{x}_{t-1}, \mathbf{y}_{1:t}; \boldsymbol{\phi}^*)$ using the reparameterization trick.

REFERENCES

- [1] R.E. Kalman, “New results in linear filtering and prediction theory,” *J. Basic Eng.*, vol. 83, pp. 95–108, 1961.
- [2] R.E. Kalman, “A new approach to linear filtering and prediction problems,” *Trans. ASME, D*, vol. 82, pp. 35–44, 1960.
- [3] M. Gruber, “An approach to target tracking,” Tech. Rep., MIT Lexington Lincoln Lab, 1967.
- [4] S.J. Julier and J.K. Uhlmann, “Unscented filtering and nonlinear estimation,” *Proceedings of the IEEE*, vol. 92, no. 3, pp. 401–422, 2004.
- [5] M. S. Arulampalam, S. Maskell, N. Gordon, and T. Clapp, “A tutorial on particle filters for online nonlinear/non-gaussian bayesian tracking,” *IEEE Transactions on Signal Processing*, vol. 50, no. 2, pp. 174–188, 2002.
- [6] D. L. Donoho, “Compressed sensing,” *IEEE Transactions on information theory*, vol. 52, no. 4, pp. 1289–1306, 2006.
- [7] A. S. Charles, A. Balavoine, and C. J. Rozell, “Dynamic filtering of time-varying sparse signals via ℓ_1 minimization,” *IEEE Transactions on Signal Processing*, vol. 64, no. 21, pp. 5644–5656, 2016.
- [8] N. Vaswani, “Kalman filtered compressed sensing,” in *2008 15th IEEE International Conference on Image Processing*. IEEE, 2008, pp. 893–896.
- [9] D. Zachariah, S. Chatterjee, and M. Jansson, “Dynamic iterative pursuit,” *IEEE Transactions on Signal Processing*, vol. 60, no. 9, pp. 4967–4972, 2012.
- [10] S.C. Patwardhan, S. Narasimhan, P. Jagadeesan, B. Gopaluni, and S.L. Shah, “Nonlinear Bayesian state estimation: A review of recent developments,” *Control Engineering Practice*, vol. 20, no. 10, pp. 933–953, 2012.
- [11] H. Coskun, F. Achilles, R. DiPietro, N. Navab, and F. Tombari, “Long short-term memory Kalman filters: Recurrent neural estimators for pose regularization,” in *Proceedings of the IEEE International Conference on Computer Vision*, 2017, pp. 5524–5532.
- [12] R.G. Krishnan, U. Shalit, and D. Sontag, “Deep Kalman filters,” *arXiv preprint arXiv:1511.05121*, 2015.
- [13] R. Krishnan, U. Shalit, and D. Sontag, “Structured inference networks for nonlinear state space models,” in *Proceedings of the AAAI Conference on Artificial Intelligence*, 2017, vol. 31.
- [14] M. Fraccaro, S. Kamronn, U. Paquet, and O. Winther, “A disentangled recognition and nonlinear dynamics model for unsupervised learning,” *Advances in NeurIPS*, vol. 30, 2017.
- [15] A. Ghosh, A. Honoré, and S. Chatterjee, “DANSE: Data-Driven Non-Linear State Estimation of Model-Free Process in Unsupervised Bayesian Setup,” in *2023 31st European Signal Processing Conference (EUSIPCO)*, 2023, pp. 870–874.
- [16] A. Ghosh, A. Honoré, and S. Chatterjee, “DANSE: Data-Driven Non-Linear State Estimation of Model-Free Process in Unsupervised Learning Setup,” *IEEE Transactions on Signal Processing*, vol. 72, pp. 1824–1838, 2024.
- [17] G. Revach, N. Shlezinger, T. Locher, X. Ni, R.J.G. van Sloun, and Y.C. Eldar, “Unsupervised learned Kalman filtering,” in *2022 30th European Signal Processing Conference (EUSIPCO)*. IEEE, 2022, pp. 1571–1575.
- [18] E.N. Lorenz, “Deterministic nonperiodic flow,” *Journal of atmospheric sciences*, vol. 20, no. 2, pp. 130–141, 1963.
- [19] S. Celikovský and G. Chen, “On the generalized lorenz canonical form,” *Chaos, Solitons & Fractals*, vol. 26, no. 5, pp. 1271–1276, 2005.
- [20] G. Chen and T. Ueta, “Yet another chaotic attractor,” *International Journal of Bifurcation and chaos*, vol. 9, no. 07, pp. 1465–1466, 1999.
- [21] O.E. Rössler, “An equation for continuous chaos,” *Physics Letters A*, vol. 57, no. 5, pp. 397–398, 1976.
- [22] J. Ko and D. Fox, “GP-BayesFilters: Bayesian filtering using Gaussian process prediction and observation models,” *Autonomous Robots*, vol. 27, pp. 75–90, 2009.
- [23] R. Frigola, F. Lindsten, T. B. Schön, and C. E. Rasmussen, “Bayesian inference and learning in gaussian process state-space models with particle mcmc,” *Advances in neural information processing systems*, vol. 26, 2013.
- [24] A. Svensson, A. Solin, S. Särkkä, and T. B. Schön, “Computationally efficient bayesian learning of gaussian process state space models,” in *Artificial Intelligence and Statistics*. PMLR, 2016, pp. 213–221.
- [25] L. Xu and R. Niu, “EKFNet: Learning system noise statistics from measurement data,” in *IEEE International Conference on Acoustics, Speech and Signal Processing (ICASSP)*. IEEE, 2021, pp. 4560–4564.
- [26] V. Garcia Satorras, Z. Akata, and M. Welling, “Combining generative and discriminative models for hybrid inference,” *Advances in NeurIPS*, vol. 32, 2019.
- [27] T. Li, Y. Song, and H. Fan, “From target tracking to targeting track: A data-driven yet analytical approach to joint target detection and tracking,” *Signal Processing*, vol. 205, pp. 108883, 2023.
- [28] S. Jung, I. Schlangen, and A. Charlish, “A mnemonic Kalman filter for non-linear systems with extensive temporal dependencies,” *IEEE Signal Processing Letters*, vol. 27, pp. 1005–1009, 2020.
- [29] H. Wen, X. Chen, G. Papagiannis, C. Hu, and Y. Li, “End-to-end semi-supervised learning for differentiable particle filters,” in *2021 IEEE International Conference on Robotics and Automation (ICRA)*, 2021, pp. 5825–5831.
- [30] L. Girin, S. Leglaive, X. Bie, J. Diard, T. Hueber, and X. Alameda-Pineda, “Dynamical variational autoencoders: A comprehensive review,” *Foundations and Trends in Machine Learning*, vol. 15, no. 1-2, pp. 1–175, 2021.
- [31] J. E. Van Engelen and H. H. Hoos, “A survey on semi-supervised learning,” *Machine learning*, vol. 109, no. 2, pp. 373–440, 2020.
- [32] X. Yang, Z. Song, I. King, and Z. Xu, “A survey on deep semi-supervised learning,” *IEEE Transactions on Knowledge and Data Engineering*, 2022.
- [33] O. Chapelle, B. Schölkopf, and A. Zien, *Semi-Supervised Learning*, The MIT Press, 1st edition, 2010.
- [34] X. Zhu and A. B. Goldberg, “Introduction to semi-supervised learning,” *Synthesis Lectures on Artificial Intelligence and Machine Learning*, 2009.
- [35] G. Kostopoulos, S. Karlos, S. Kotsiantis, and O. Ragos, “Semi-supervised regression: A recent review,” *Journal of Intelligent & Fuzzy Systems*, vol. 35, no. 2, pp. 1483–1500, 2018.
- [36] K. Cho, B. van Merriënboer, D. Bahdanau, and Y. Bengio, “On the properties of neural machine translation: Encoder–decoder approaches,” in *Proc. of 8th workshop, SSST-8*, 2014, pp. 103–111.
- [37] C. M. Bishop and N. M. Nasrabadi, *Pattern recognition and machine learning*, vol. 4, Springer, 2006.
- [38] S. Hochreiter and J. Schmidhuber, “Long short-term memory,” *Neural computation*, vol. 9, no. 8, pp. 1735–1780, 1997.
- [39] A. Paszke et al., “PyTorch: An imperative style, high-performance deep learning library,” *Advances in NeurIPS*, vol. 32, 2019.
- [40] D.P. Kingma and J. Ba, “Adam: A method for stochastic optimization,” in *3rd International Conference on Learning Representations (ICLR)*, 2015.
- [41] R. Labbe, “FilterPy - Kalman and Bayesian filters in Python,” URL: <https://filterpy.readthedocs.io/en/latest/>, 2018.
- [42] Ian Goodfellow, Yoshua Bengio, and Aaron Courville, *Deep learning*, MIT press, 2016.
- [43] P. J. Werbos, “Backpropagation through time: what it does and how to do it,” *Proceedings of the IEEE*, vol. 78, no. 10, pp. 1550–1560, 1990.
- [44] D. P. Kingma and M. Welling, “Auto-encoding variational bayes,” in *2nd International Conference on Learning Representations, (ICLR)*, Yoshua Bengio and Yann LeCun, Eds., 2014.